Experimental Study on Hysteretic Behaviour of Welded Stainless Steel Box-section Columns

KY Ning[a], L Yang[a], HY Ban[b], MH Zhao[a], YN Sun[a]

The College of Architecture and Civil Engineering, Beijing University of Technology, Beijing, China[(a)],
Tsinghua University, Beijing, China[(b)]

Abstract

Eight specimens were tested under cyclic loading to investigate hysteretic behaviour of welded stainless steel box-section columns. Failure modes, bearing capacities, energy dissipation and ductility of the specimens were studied, and influence of the width-to-thickness ratio as well as the axial-load ratio on hysteretic behaviour was also analysed. The test results indicate that the welded stainless steel box-section columns possess good seismic performance and energy dissipation capacities. With larger width-to-thickness ratios, the hysteresis curve becomes less plump. The larger the axial-load ratio is, the smaller the maximum bearing capacity becomes and the faster the bearing capacity declines.

Keywords

Stainless steel; Box-section column; Hysteretic behaviour; Seismic performance; Width-to-thickness ratio

1   Introduction

Due to its high strength, good toughness and excellent plastic deformation, steel structure exhibits excellent seismic performance and is widely used in building structures. However, with continuous development of the steel structure, disadvantage of ordinary steel in construction applications has been highlighted. There are many drawbacks in ordinary steel, for example, it can-not resist high temperature, it is easy to rust in corrosion resistance, which leads to huge maintenance costs and relevant safety issues[1-3]. Stainless steel, nevertheless, is able to make up for these deficiencies. Being added more than 10.5% of chromium in its material, stainless steel has excellent corrosion resistance. Moreover, it has excellent fire resistance, high ductility, less maintenance and low whole-life costs[4-9] therefore application of the stainless steel in building structures is becoming more and more extensive.

In recent years, scholars did numerous research on the stainless steel, mainly focusing on properties of material[10], members[11-21], connections[22-25] and residual stress of section[26-27]. However, hysteretic behaviour of stainless steel was less studied. Few research works focused on the hysteretic behaviour of stainless steel material[28-29], and a gap was found in studying the hysteretic behaviour of at the level of structural members. In view of the growing use of stainless steel in the construction industry across the world, the hysteretic behaviour of welded stainless steel box-section columns should be fully studied. In order to avoid the rapid degradation of stiffness and strength of the columns caused by local buckling of flange plates or web plates, the width-to-thickness ratio of the ordinary steel box-section columns in seismic areas shall not exceed the limiting values specified in ANSI/AISC 341–10[30] , Eurocode 3[31] and GB 50011(2010)[32]. Since there is a great difference in material properties between stainless steel and ordinary steel, and this difference could greatly impact the hysteretic behaviour of structural members, hysteretic behaviour of welded stainless steel box-section columns needs to be investigated to provide bases of design suggestions. Whether the limiting values of width-to-thickness ratios prescribed in current national standards are applicable for stainless steel is also needed to be clarified.

In order to investigate the hysteretic behaviour of welded stainless steel box-section columns and to better promote the application of stainless steel in building structures, four austenitic and four duplex welded stainless steel box-section columns were tested under cyclic horizontal loading. The hysteretic behaviour was evaluated and analysed by hysteresis curves, skeleton curves, energy dissipation coefficients and ductility coefficients.

2   Experimental Program

2.1   Material tests

Material tests in this study were undertaken according to Chinese specification GB/T228.1(2010)[33], and the tensile coupons were cut directly from the raw stainless steel hot-rolled sheets, which were the same batch with that of the specimens. The test material included Grades EN 1.4301 (corresponding to type 304 in the ASTM system) and EN 1.4462 (corresponding to type 2205 in the ASTM system), which are widely used in constructions. For each material grade with different thicknesses (nominal thicknesses were 6 mm, 8 mm and 10 mm), three coupons were prepared along the rolling direction.

The average measured material parameters are summarised in Table 1, where t is the measured thickness, $f_{0.2}$ is the 0.2% proof stress, f_u is the ultimate tensile stress, E_0 is the elastic modulus, n represents the strain-hardening exponent and A^* is the percentage elongation after fracture. The tensile stress–strain curves were calculated on the basis of the measured load-displacement curves, as plotted in Fig. 1(a) and (b) for austenitic and duplex stainless steel respectively.

**Table 1   Average measured tensile material properties**

Grades	t(mm)	E_0 (MPa)	$f_{0.2}$(MPa)	f_u(MPa)	A^* (%)	n
Austenitic	5.82	205000	304.0	707.0	53.0	6.5
	7.82	200000	284.0	689.3	54.6	6.0
	9.60	210000	358.0	704.7	53.2	6.6
Duplex	5.75	230000	630.0	794.0	28.1	7.0
	7.70	230000	595.0	763.7	30.9	7.5
	9.70	215000	567.0	754.0	34.9	8.5

(a) Austenitic stainless steel   (b) Duplex stainless steel
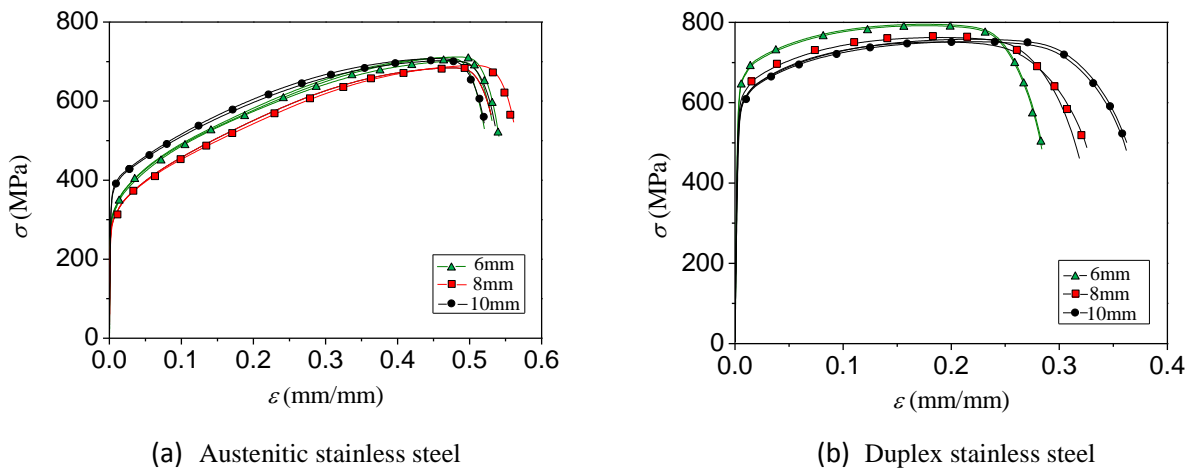
Fig. 1 Measured stress-strain curves of stainless steel

2.2   Specimen fabrication

The test is based on the assumption that the column inflection point is located at the mid-height of the column to design the specimens, which can be therefore simplified as a member of a half-height of the column with one end being fixed and the other being hinged in vertical direction and being movable in horizontal direction. The overall dimensional diagram and details of the fixed end for the specimens are shown Fig. 2. The processing height of all specimens was 1860 mm including a 30 mm-thick top end plate and a 30 mm-thick bottom end plate. To ensure sufficient stiffness of the fixed end and to avoid potential welding failure of the box section at the column base, stiffening plates were welded at the fixed end. Q345 steel was used for all the stiffening plates with 300 mm height and 12 mm thickness as well as for the top and bottom end plates, as shown in Figs. 2(b) and (c). Detailed specimen parameters are shown in Table 2, and all the eight specimens were equilateral box- section. In Table 2, B and t_w represent respectively the width of the box-section and the thickness of the plate, h represents the height of the web, $h= B-2t_w$, and $[h/t_w]$ represents the limiting values of width-to-thickness ratio of the stainless steel box-section columns for seismic level 1 calculated according to Chinese specification GB 50011(2010). In addition, N represents the axial load constantly applied to the specimens and N_0 represents the axial-load ratio (i.e. $N/f_{0.2}A$).
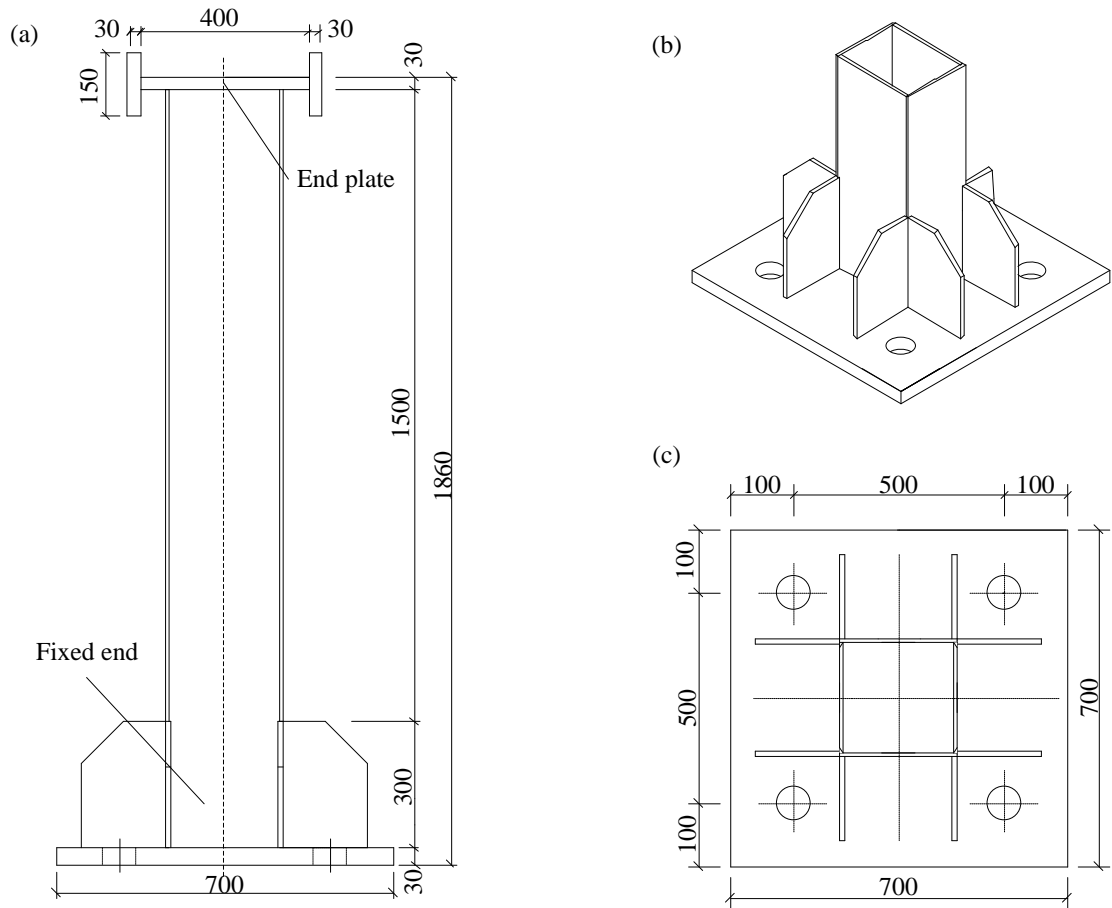
Fig. 2 Design of specimens(Unit:mm). (a) geometrical details; (b) 3-D of fixed end with stiffening plates; (c) plan view of fixed end with stiffening plates

Table 2 Measured geometry of specimens and axial-load ratios

Cross-section	Specimens	B / mm	t_w /mm	h/t_w	$[h/t_w]$	N_0	N(KN)
	B304-1	280.0	9.60	26.0	35.3	0.2	443
	B304-2	279.0	7.85	33.0	35.3	0.2	357
	B304-3	280.0	7.85	33.0	35.3	0.4	714
	B304-4	281.0	5.82	44.7	35.3	0.2	270
	B2205-1	200.5	9.70	18.0	23.8	0.2	684
	B2205-2	198.0	7.70	23.0	23.8	0.2	553
	B2205-3	198.0	7.70	23.0	23.8	0.4	1106
	B2205-4	198.5	5.75	31.3	23.8	0.2	419

2.3 Test setup and measurement arrangement

The test setup is shown in Fig. 3 and Fig. 4, and the vertical load was applied by a 1500 KN hydraulic jack and the horizontal load was applied by a 500 KN hydraulic actuator. The vertical load was applied at the top end plate of the column, and the horizontal load was applied at the horizontal loading plate, which was arranged at both ends of the column end plate to connect with the horizontal actuator. The actual height L_0 of the test specimen is 1515 mm from the edge of the stiffening plate to the centre of the top end plate.
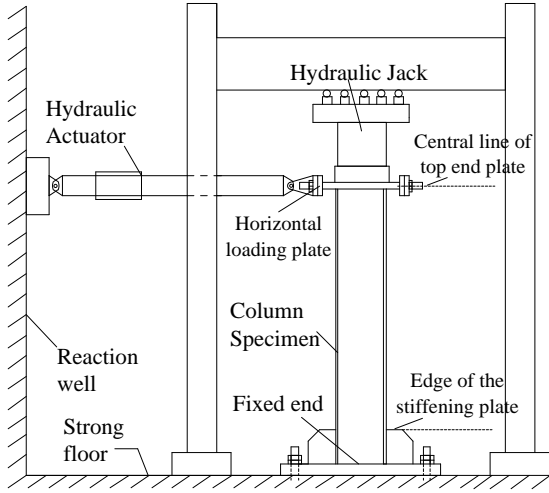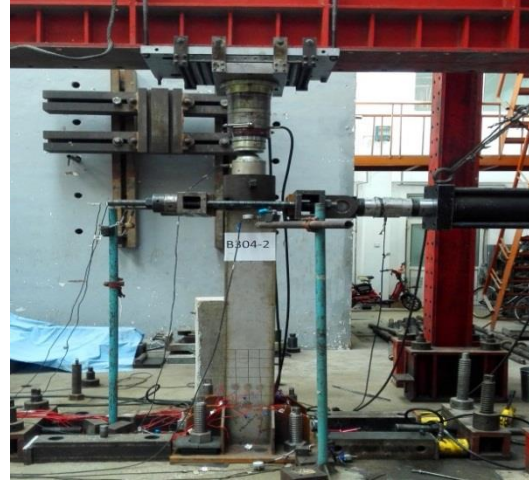
Fig. 3 Schematic diagram of test setup　　　　　　　　Fig. 4 Test photo

Arrangement of the measuring points is shown in Fig. 5, mainly including the arrangement of linear varying displacement transducers (LVDTs) and strain gauges. Twelve strain gauges were affixed at sections 1-1 and 2-2, respectively, for the measurement of strain in the column area. Eight LVDTs were arranged to monitor the column top displacement and the rigidity condition of the column bases. The in-plane horizontal displacement of the column top was measured by LVDT D1 and D2. LVDT D3 and D6 were respectively used to measure the out-of-plane horizontal displacement of the top of the column and the column base. LVDT D4 and D5 were used to record the rotating condition of the column base. LVDT D7 and D8 were used to record the in-plane slipping of the column base.
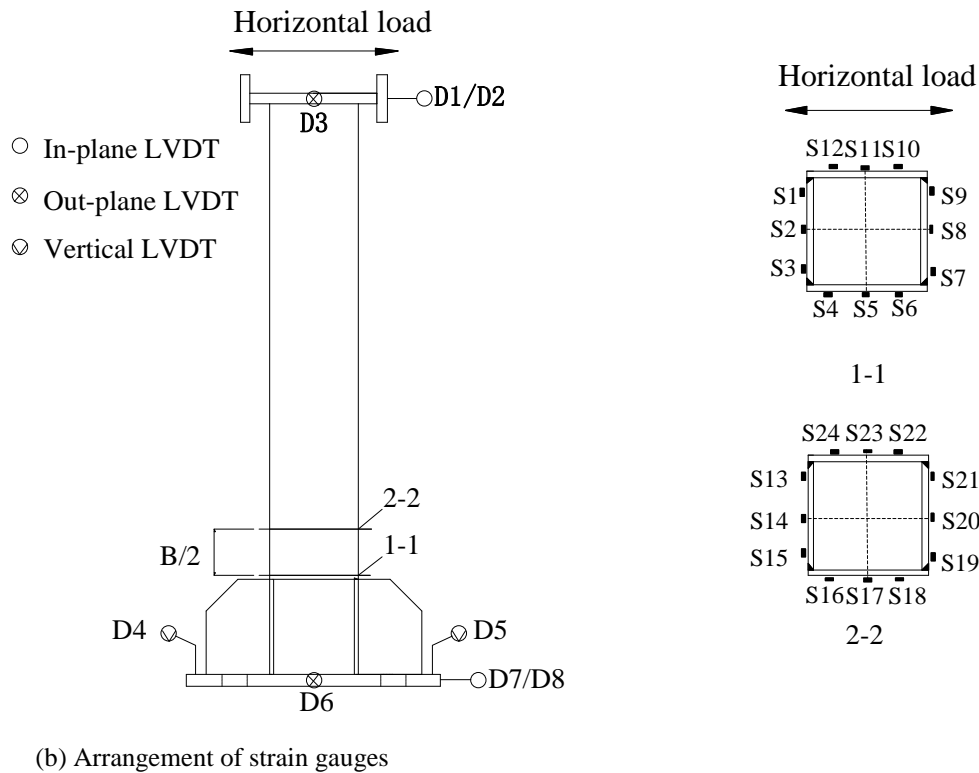

(b) Arrangement of strain gauges

Fig. 5 Measurement points

2.4 Loading protocol

The test loading protocol was defined according to Chinese specification JGJ 101-96(1997)[34]. First, the target vertical load was exerted on specimens by hydraulic jacks and was kept constant throughout the entire testing process. Then, the horizontal load was applied to the top of the column, and controlled by the displacement control. Under the combined action of axial force and bending moment, the yielding displacement δ_y in horizontal was calculated according to the yielding criterion of outmost fibre, i.e. Eq (1), where $f_{0.2}$ is the 0.2% proof stress, N is axial load and A is section area, L_0 is actual height of the test specimen, E_0 is the elastic modulus, y is half height of the section, and the calculation

4

results are shown in Table 3. The first load step was taken as the displacement $0.5\delta_y$ with one cycle. Then, the second load step was taken as the displacement δ_y with three cycles. And in the following load steps, δ_y was taken as the displacement increase (i.e. $\pm 2\delta_y$, $\pm 3\delta_y$, $\pm 4\delta_y$ ...), and each step was also repeated three times until failure occurred, as shown in Fig.6. According to Chinese specification JGJ 101-96(1997), the final failure of specimen is defined when the bearing capacity of the specimen is reduced to less than 85% of the maximum bearing capacity.

$$\delta_y = \frac{(f_{0.2} - N/A)L_0^2}{3E_0 y} \tag{1}$$

Table 3 Yielding displacement

Specimens	B304-1	B304-2	B304-3	B304-4	B2205-1	B2205-2	B2205-3	B2205-4
δy(mm)	8	7	6	7	17	17	14	18

(a) Arrangement of LVDTs
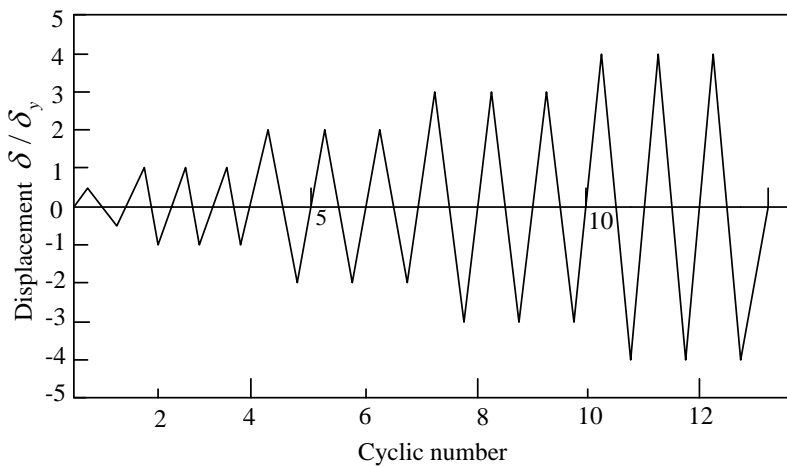
Fig. 6 Cyclic loading protocol

3   Test Results

3.1   Test phenomena and failure mode

When the specimen B304-1 was loaded to the first circle of the $6\delta_y$ displacement level, local buckling in the flange began to appear, and the buckling deformation was half sine-wave and slightly convex outwards. The maximum buckling deformation occurred at 160 mm from the edge of the stiffening plate. When the displacement load continued to be applied to the second circle, the horizontal load reached its maximum value, and then the buckling deformation did not recover when the displacement reduced to zero. When the load was loaded to the first circle of the $7\delta_y$ displacement level, the deformation range of the flange was expanded and local buckling in the web began to appear. The buckling deformation of web was also half sine-wave but concave inwards, and the buckling deformation range was within 270 mm, and the maximum deformation occurred at 160 mm from the edge of the stiffening plate. At the load step of the first circle of the $8\delta_y$ displacement level, the load dropped to 79% of the maximum bearing capacity, and the specimen was broken. After loading into the second circle of the $8\delta_y$ displacement level, the load dropped to 77% of the maximum bearing capacity, and the load stopped.

The test phenomena of the other specimens were generally similar to that of the specimen B304-1. The failure process was firstly the local buckling deformation of the flange, then the local buckling of the web and the bearing capacity dropped to less than 85% of the maximum one. The failure modes are shown in Fig. 7, where the local buckling shape of specimen B304-2 was different, the flange was concave in half sine-wave inwards, and the web was half sine-wave convex outwards. The local buckling shape of other specimen were similar to that f B304-1, the flange was half sine-wave convex outwards, and the web was half sine-wave concave inwards. The failure process of all the test specimens is shown in Table 4, where the buckling deformation value is the average of the flange and web, D_l represents the displacement level corresponding to local buckling, and D_{max} and D_u represent the displacement levels corresponding to the maximum bearing capacity and failure load respectively. The numbers in bracket denote the number of loading cycles at the corresponding displacement level.

(a) B304-1   (b) B304-2   (c) B304-3   (d) B304-4

(e) B2205-1   (f) B2205-2   (g) B2205-3   (h) B2205-4
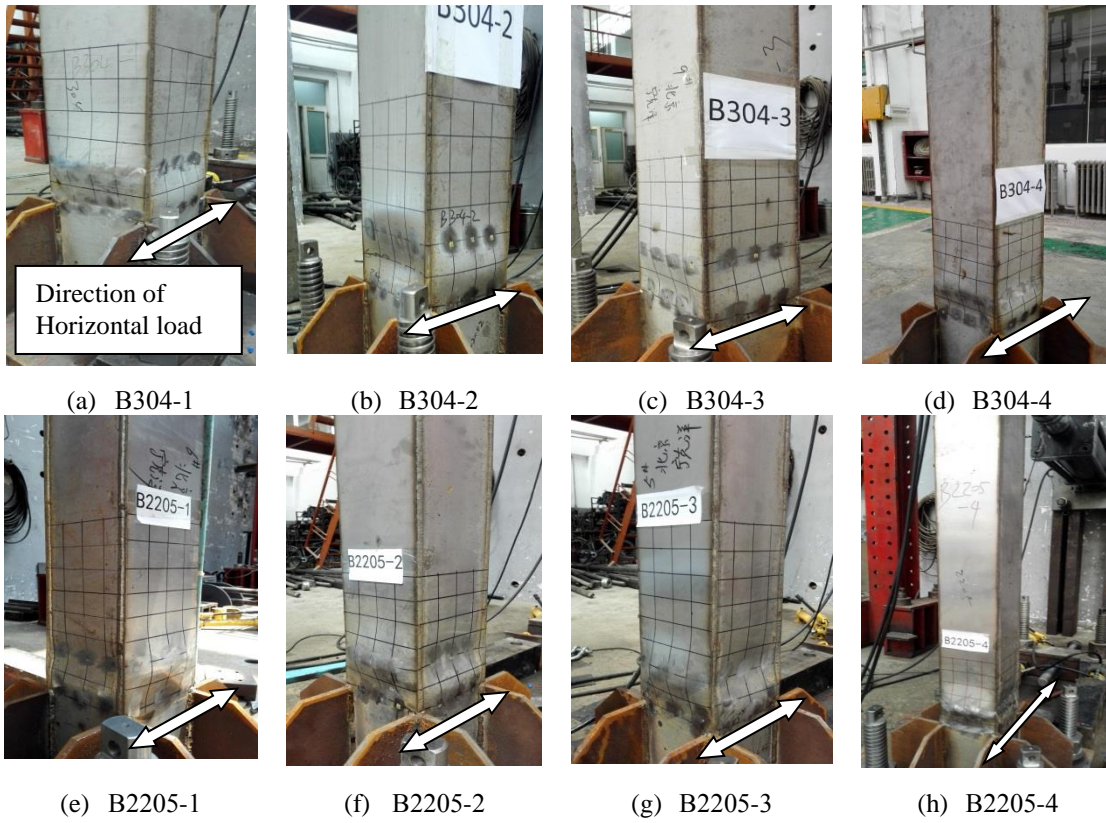
Fig.7 Failure modes of specimens

Table 4 Failure processes of specimens

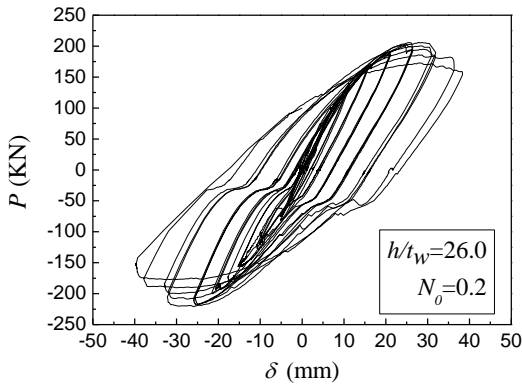| Specimens	D_l	D_{max}	D_u	Buckling range	Maximum deformation position
B304-1	$6\delta_y$ (1)	$6\delta_y$ (2)	$8\delta_y$ (1)	0.91B	0.51B
B304-2	$6\delta_y$ (1)	$6\delta_y$ (2)	$7\delta_y$ (1)	0.87B	0.40B
B304-3	$5\delta_y$ (1)	$5\delta_y$ (2)	$6\delta_y$ (1)	0.87B	0.50B
B304-4	$4\delta_y$ (1)	$4\delta_y$ (1)	$5\delta_y$ (1)	1.13B	0.50B
B2205-1	$5\delta_y$ (2)	$5\delta_y$ (2)	$6\delta_y$ (3)	0.93B	0.43B
B2205-2	$5\delta_y$ (1)	$5\delta_y$ (1)	$5\delta_y$ (2)	B	0.50B
B2205-3	$5\delta_y$ (1)	$5\delta_y$ (1)	$5\delta_y$ (1)	B	0.50B
B2205-4	$3\delta_y$ (2)	$4\delta_y$ (1)	$4\delta_y$ (2)	1.13B	0.50B

3.2 Hysteresis curves

The load-displacement hysteresis curves of the eight test specimens are shown in Fig. 8, and the ordinate is the horizontal load (P), and the abscissa is the corresponding horizontal displacement (δ). Under the action of cyclic load, especially when the horizontal load is large, the connecting bolts of the column base are prone to loose, so the horizontal displacement should eliminate the influence of the rigid rotation and slipping of the base, and the horizontal displacement can be calculated on the basis of Eq (2), where R_{D1} and R_{D2} are readings of LVDT D1 and D2 respectively, R_{D7} and R_{D8} are readings of LVDT D7 and D8 respectively, R_{D4} and R_{D5} are readings of LVDT D4 and D5 respectively, 700 is the distance between LVDT D4 and D5, 1815 is the distance from the bottom end plate to the centre of the top end plate. According to the hysteresis curve and Table 4, the following characteristics can be obtained:
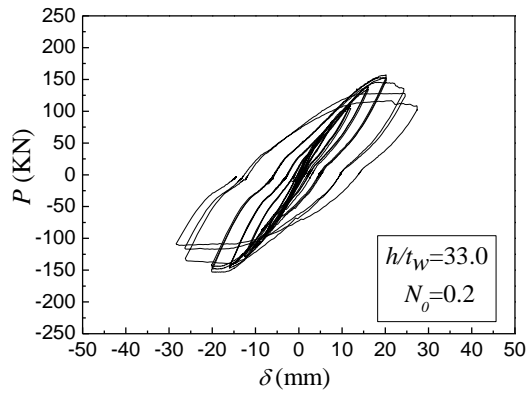
(1) The hysteresis curves of all the specimens are spindle-shaped, and there is no obvious pinch phenomenon, and the plumpness of hysteresis curve of each specimen decreases with the increase of width-to-thickness ratio.

(2) The range of plate buckling was within 0.87B to 1.13B and the position of the buckling center with the maximum local deformation was 0.40B to 0.51B from the edge of the stiffening plate.

(3) According to the experimental phenomenon, it can be seen that when the width-to-thickness ratio is much smaller than the seismic limit, the specimen undergoes sufficient plasticity when the specimen fails, and local buckling occurs later. When the width-to-thickness ratio is much larger than the seismic limit, local buckling occurs earlier and specimen bearing capacity in late period declines rapidly. As width-to-thickness ratio increases, local buckling occurs at a lower displacement level, and the displacement levels corresponding to the maximum bearing capacity and failure load are both smaller.

(4) By comparing the specimens B304-2 with B304-3 and B2205-2 with B2205-3, it can be seen that the axial-load ratio has great influence on the maximum bearing capacity of the stainless steel column. As axial-load ratio increases, the maximum bearing capacity decreases.
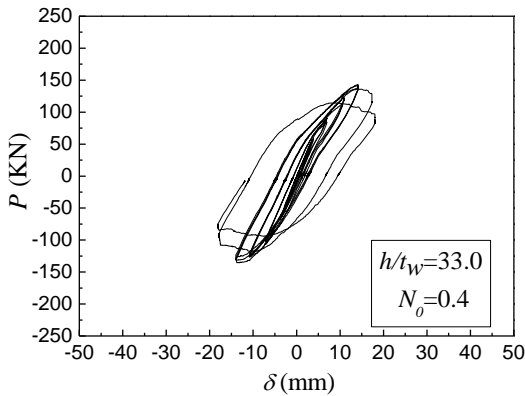
$$\delta = \frac{R_{D1} + R_{D2}}{2} - \frac{R_{D7} + R_{D8}}{2} - 1815\left(\frac{R_{D4} - R_{D5}}{700}\right) \tag{2}$$

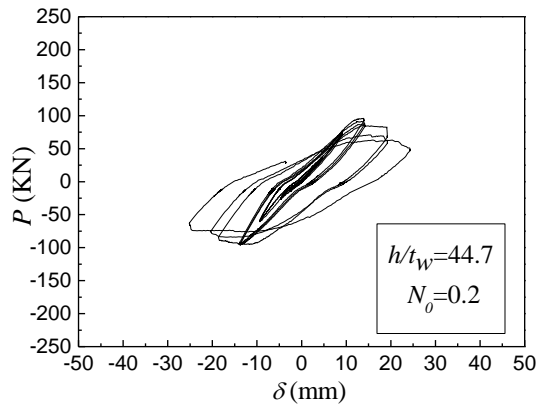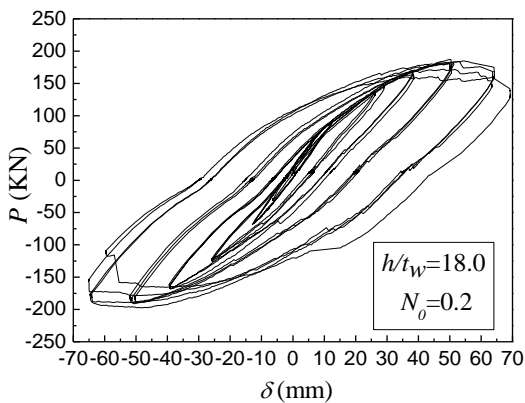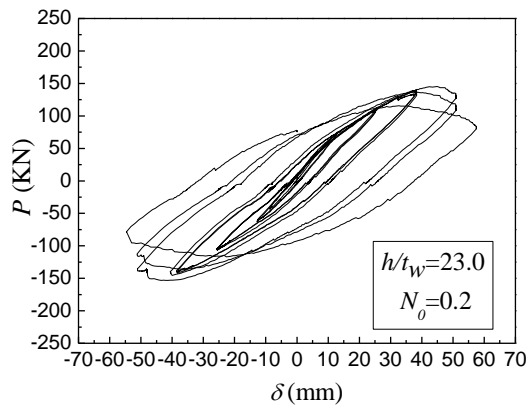(a)B304-1

(b)B304-2

(c)B304-3

(d)B304-4

(e)B2205-1

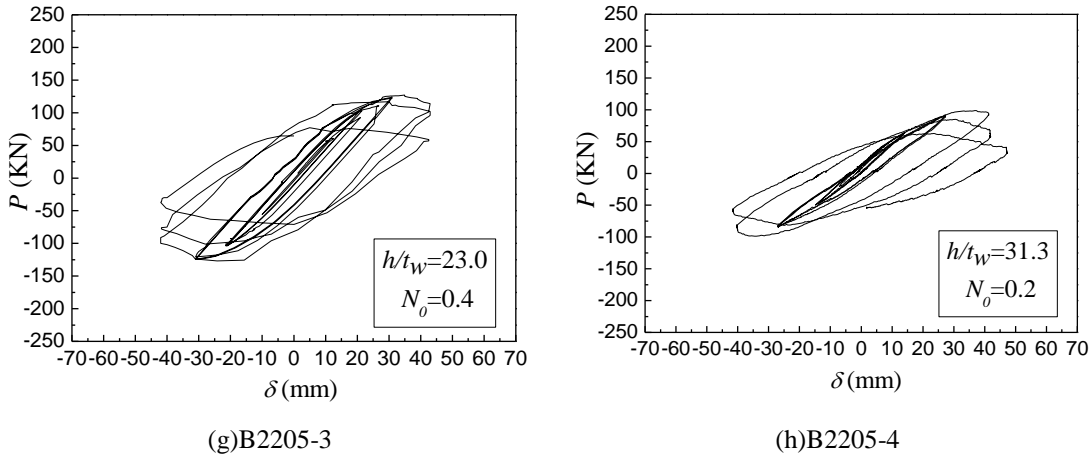(f)B2205-2

(g)B2205-3 (h)B2205-4

Fig. 8 Hysteresis curves of specimens

4 Result Analysis

4.1 Energy dissipation capacity

Energy dissipation capacity of the specimen, an important index to evaluate the seismic performance, can be evaluated qualitatively by the plumpness of hysteresis curve. The plumper the hysteresis curve is, the better the seismic performance is. In addition, the energy dissipation coefficient E can also be used as an evaluation index. As shown in Fig. 10, the energy dissipation coefficient E is calculated on the basis of Eq (3) where $S_{(FBE+FCE)}$ represents the area enclosed by curve of FBE and FCE and $S_{(AOB+COD)}$ is the sum of area of triangle of AOB and COD as illustrated in Fig. 9[35].

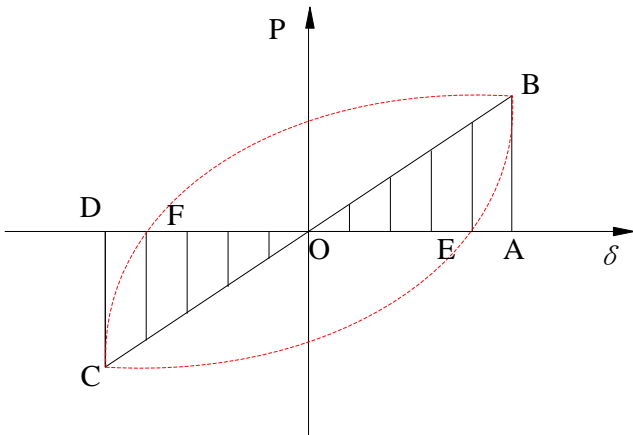$$E = \frac{S_{(FBE+FCE)}}{S_{(A0B+COD)}}$$ (3)
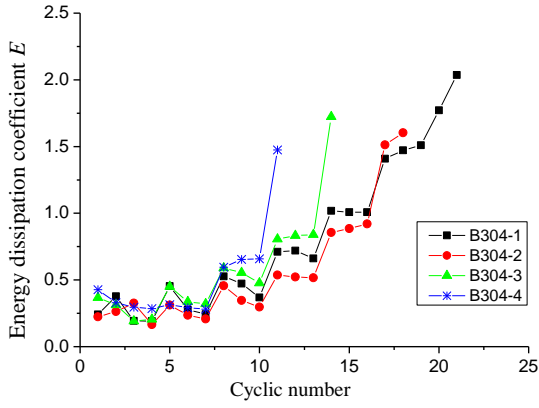

Fig. 9 P-δ Hysteresis curve

Energy dissipation coefficients from the first cycle at each loading step until failure for all the specimens are shown in Fig. 10 and Fig. 11. It can be seen that for each specimen, the energy dissipation coefficient increases as the displacement level increases due to larger plastic deformation.

Fig. 10 Energy dissipation coefficients of austenitic stainless steel specimens
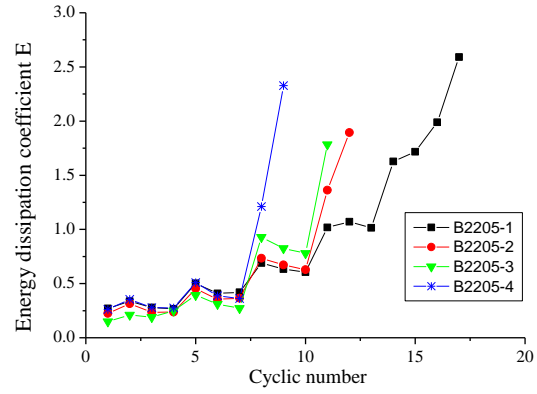
Fig. 11 Energy dissipation coefficients of duplex stainless steel specimens

It can be seen from Fig. 10 that, for austenitic stainless steel specimen, energy dissipation coefficient of specimen B304-1 in the loading cycle of failure is obviously larger than those of the other specimens due to its smallest width-to-thickness ratio. The width-to-thickness ratio of B304-2 is larger than that of B304-1, and the loading displacement level is close. It can be seen that the energy dissipation coefficient of B304-1 is obviously stronger than that of B304-2 before the specimen reaches the maximum bearing capacity. Specimen B304-4 with largest width-to-thickness ratio experiences least number of circles before failure, and its energy dissipation coefficient is stronger than that of the other specimens after the specimen reaches the maximum bearing capacity and increases rapidly in the last cycle of loading as shown in Fig.10. The main reason for the above phenomenon is that the 304 specimen enters the plastic stage ahead of the other specimen and the horizontal load decreases sharply with the increase of the displacement after the peak load. For specimens B304-2 and B304-3 with the same dimension while different axial-load ratio, the axial-load ratio of specimen B304-3 is increased by 100% compared with that of specimen B304-2. The number of circles experienced by specimen B304-2 before failure is significantly greater than that of specimen B304-3, and the energy dissipation coefficient of the specimen B304-3 increases rapidly in the last cycle of loading.

It can be seen from Fig. 11 that the change regulation is similar to that of austenitic stainless steel specimens for duplex stainless steel specimens. Specimen B2205-1 with smallest width-to-thickness ratio experiences largest number of circles before failure, and its energy dissipation coefficient of the loading cycle of failure is the largest.
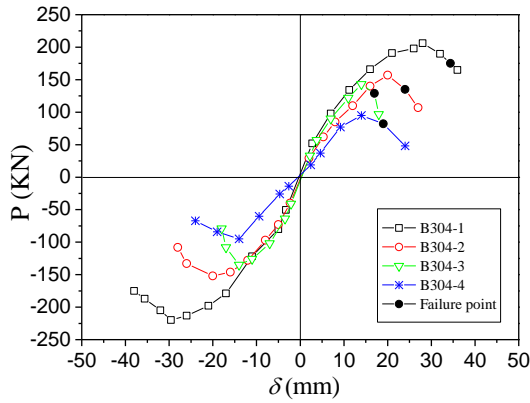
4.2   Skeleton curve and ductility

Skeleton curve is the envelope obtained by connecting the peak points on the measured hysteresis curve together, which can reflect the relationship between the load and displacement of the specimen, as well as stiffness and ductility. According to the hysteresis curve of Fig. 6, the load-displacement (P-δ) skeleton curves of the specimen are shown in Fig. 13 and Fig. 14, where failure point is the point corresponding to the horizontal load falling to 85% of the peak value. The displacement ductility coefficient (μ) is adopted in this paper to assess the ductility of welded stainless steel box-section columns, where μ can be defined as Eq. (4). In Eq. (4), Δ_y and Δ_u = lateral displacements at column yield and failure respectively, as shown in Fig. 12. The peak load (P_{max}), deformation and ductility coefficient are summarised in Table 5.
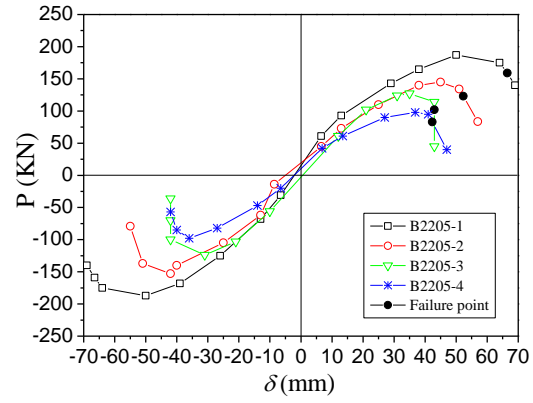
$$\mu = \Delta_u/\Delta_y \qquad\qquad (4)$$
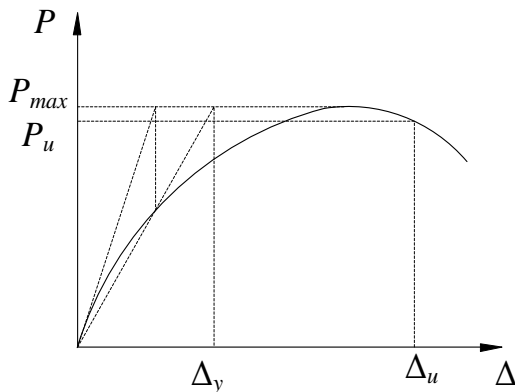
Fig. 12. Typical P – Δ skeleton curve

Fig. 13 Cyclic skeleton curves of austenitic stainless steel specimens

Fig. 14 Cyclic skeleton curves of duplex stainless steel specimens

As shown in Fig. 13, Fig. 14 and Table 5, the elastic stiffness, peak load and ductility coefficients of each specimen decrease with an increase of the width-to-thickness ratio, and for specimens with the same dimension while different axial-load ratio, the larger the axial-load ratio is, the smaller the peak load ,elastic stiffness and ductility coefficient are.

Table 5 Peak load, deformation and ductility coefficient

Specimens	P_{max}/KN	Δ_y/mm	Δ_u/mm	μ
B304-1	206	17.23	34.4	1.995
B304-2	157	15.58	24.0	1.540
B304-3	143	12	15.9	1.325
B304-4	95	12.7	19.0	1.496
B2205-1	187	36.84	66.5	1.805
B2205-2	145	34.25	52.3	1.527
B2205-3	127	31.06	43.0	1.387
B2205-4	98	28.5	42.3	1.489

Based on Fig. 13, the width-to-thickness ratio[26] of the specimen B304-1 is significantly smaller than the seismic specification limit, and its elastic stiffness, peak load and ductility coefficient are the largest. The specimen B304-1 reaches the peak load in the second circle at the displacement level of $6\delta_y$, then the degradation of the bearing capacity and rigidity is slow and the failure is achieved in the first circle at the displacement level of $8\delta_y$. The plastic deformation and ductility of the specimen are fully developed and the hysteresis curve is plump, and specimen B304-1 exhibits good seismic performance. The width-to-thickness ratio (44.7) of the specimen B304-4 is significantly larger than the seismic specification limit, and its elastic stiffness and peak load are the smallest. The specimen B304-4 reaches the peak load in the first circle at the displacement level of $4\delta_y$, then the degradation of the bearing capacity and rigidity is fast and the failure is achieved in the first circle at the displacement level of $5\delta_y$. The plastic deformation and ductility of the specimen are less developed. For specimens B304-2 and B304-3 with the same dimension while different axial-load ratio, specimen B304-2 reaches the peak load and failure in the second circle at the displacement level of $6\delta_y$ and in first circle at the displacement level of $7\delta_y$, respectively, and specimen B304-3 reaches the peak load in the second circle at the displacement level of $5\delta_y$, then the degradation of the bearing capacity is rapid and the failure is achieved in the first circle at the displacement level of $6\delta_y$. Comparing the specimens B304-2 and B304-3, the axial-load ratio of specimen B304-3 is increased by 100% compared with that of specimen B304-2, but the peak load is decreased by 9% and ductility coefficient is decreased by 18%. In addition, a higher axial-load ratio of B304-3 also introduced a more rapid bearing capacity degradation after the peak load in the skeleton curve, than that of specimen B304-2.

As can be seen from Fig. 14, the change regulation of the skeleton curve of the duplex stainless steel specimens is similar to that of the austenitic stainless steel specimens. The width-to-thickness ratio of the specimen B2205-1 is the smallest, and its elastic stiffness and peak load are the largest. And from comparison of specimens B2205-1, B2205-2 and B2205-4, it is evident that under the same axial-load ratio, the elastic stiffness, peak load and ductility coefficient are determined by the width-to-thickness ratio, and the larger the width-to-thickness ratio is, the faster the bearing capacity and rigidity degenerate. By comparing specimens B2205-2 and B2205-3, it is known that for specimens with same width-to-thickness ratio, axial-load ratio has few effects on elastic stiffness but significant influence on the peak load. For example, the axial-load ratio of specimen B2205-3 is increased by 100% compared with that of specimen B2205-2, resulting in a decrease of 12.4% for the peak load.

5 Conclusions

Experimental study on hysteretic behaviour of welded stainless steel box-section columns is introduced in this paper. Four austenitic and four duplex welded stainless steel box-section columns were tested under cyclic loading to investigate the hysteretic behaviour. The hysteretic behaviour was evaluated and analysed by hysteresis curves, skeleton curves, energy dissipation coefficients and ductility coefficients. Conclusions can be drawn as follows.

- The welded box-section stainless steel columns have good seismic performance and energy dissipation capacity, the plasticity development of the specimen is sufficient, and the hysteretic curve of the specimen is plump.

- For the specimens with the same axial-load ratio, as width-to-thickness ratio increases, local buckling occurs at a lower displacement level, and the displacement levels corresponding to the maximum bearing capacity and failure load are both smaller.

- All the specimens showed local buckling first at flange and then at web when subjected to cyclic horizontal load. The range of buckling was within 0.87B to 1.13B and the position of the buckling center with the maximum local deformation was 0.40B to 0.51B from the edge of the stiffening plate.

- With an increase of width-to-thickness ratio or axial-load ratio, the plumpness of hysteric curve, energy dissipation capacity, ductility of specimens and maximum bearing capacity decreased. In addition, the larger width-to-thickness ratio or axial-load ratio is, the faster the bearing capacity and rigidity degenerate.

- In this paper, only width-to-thickness ratio and axial-load ratio are considered in the test, other influence factors, including column slenderness ratio, should be studied in the future.

Acknowledgement

References

[1] Melchers R E. Corrosion uncertainty modelling for steel structures. Journal of Constructional Steel Research, 1999, 52(1): 3-19.

[2] Ma Jian, Wang Meng, Sun Xuejun. Steel structure corrosion present situation and protection development. Building Structure, 2009(39): 344-345(in Chinese)

[3] Houska C. Stainless steel in Architecture, Building & Construction: Guidelines for corrosion prevention. Nickel Development Institute, Publication 11024, 44 pages, 2001

[4] Vaghani M, Vasanwala S A. Stainless Steel As A Structural Material: State Of Review. International Journal of Engineering Research & Applications, 2014, 4(3).

[5] Wu Mingyu, Hu Kai, Li Yungang. Research progress of Cr-Ni austenitic stainless steels. Foundry Technology, 2016 (37): 1079-1084(in Chinese).

[6] EN 10088-2. Stainless steels. Technical delivery conditions for sheet/plate and strip of corrosion resisting steels for general purposes. Brussels: European Committee for Standardization (CEN); 2005.

[7] Leroy Gardner BEng MSc PhD DIC CEng MICE. The use of stainless steel in structures. Progress in Structural Engineering & Materials, 2010, 7(2):45-55.

[8] Kahl S. Stainless and Stainless-Clad Reinforcement for Highway Bridge Use. Clad Metals, 2012.

[9] Harold M. Cobb. The history of stainless steel. ASM International, USA, 2010.

[10] Gardner L, Bu Y, Francis P, P. Francis, N.R. Baddoo, K.A. Cashell, F. McCann. Elevated temperature material properties of stainless steel reinforcing bar. Construction and Building Materials, 2016, 114:977-997.

[11] Anbarasu M, Ashraf M. Behaviour and design of cold-formed lean duplex stainless steel lipped channel columns. Thin-Walled Structures, 2016, 104:106-115.

[12] Yang L, Zhao M H, Chan T M, Shang F, Xu D C. Flexural buckling of welded austenitic and duplex stainless steel I-section columns. Journal of Constructional Steel Research, 2016, 122:339-353.

[13] Yang L, Zhao M H, Xu D C, Shang F, Yuan H X, Wang Y Q, Zhang Y. Flexural buckling behavior of welded stainless steel box-section columns. Thin-Walled Structures, 2016, 104:185-197.

[14] Yang L, Shi G, Zhao M H, Zhou W J. Research on interactive buckling behaviour of welded steel box-section columns. Thin-Walled Structures, 2017, 115: 34-47.

[15] Gardner L, Bu Y, Theofanous M. Laser-welded stainless steel I-sections: Residual stress measurements and column buckling tests. Engineering Structures, 2016, 127:536-548.

[16] Anwar-Us-Saadat M, Ashraf M, Ahmed S. Behaviour and design of stainless steel slender cross-sections subjected to combined loading. Thin-Walled Structures, 2016, 104:225-237.

[17] Zhao O, Rossi B, Gardner L, et al. Behaviour of structural stainless steel cross-sections under combined loading – Part I: Experimental study. Engineering Structures, 2015, 89:236-246.

[18] Zhao O, Rossi B, Gardner L, et al. Behaviour of structural stainless steel cross-sections under combined loading – Part II: Numerical modelling and design approach. Engineering Structures, 2015, 89:247-259.

[19] Zhao O, Gardner L, Young B. Structural performance of stainless steel circular hollow sections under combined axial load and bending – Part 1: Experiments and numerical modelling. Thin-Walled Structures, 2015, 101:231–239.

[20] Zhao O, Gardner L, Young B. Structural performance of stainless steel circular hollow sections under combined axial load and bending – Part 2: Parametric studies and design. Thin-Walled Structures, 2015, 101:240–248.

[21] Zhao O, Gardner L, Young B. Buckling of ferritic stainless steel members under combined axial compression and bending. Journal of Constructional Steel Research, 2016, 117:35-48.

[22] Cai Y, Young B. Bearing factors of cold-formed stainless steel double shear bolted connections at elevated temperatures. Thin-Walled Structures, 2015.

[23] L. Yang, Y.Q. Wang, J. Guan, Bearing strength of stainless steel bolted connections, Adv. Struct. Eng. 18 (7) (2015) 1051–1062.

[24] Salih E L, Gardner L, Nethercot D A. Bearing failure in stainless steel bolted connections. Steel Construction, 2011, 33(2):549-562.

[25] Salih, Mohamed E L. Analysis and design of stainless steel bolted connections. Imperial College London, 2010.

[26] Wang Yuanqing, Yuan Huanxin, Shi Yongjiu, Shu Ganping, Liao Dongfan. Measurement and distribution models of residual stresses in welded stainless steel box sections. Journal of Southeast University (Natual Science Edition), 2013. 43(5):979-985(in Chinese).

[27] Howlader M K, Marik J, Jandera M. Cold-forming effect on stainless steel sections. International Journal of Steel Structures, 2016, 16(2):317-332.

[28] Wang Meng, Yang Guowei, Wang Yuanqing, Chang Ting, Shi Yongjiu. Study on hysteretic constitutive model of austenitic stainless steels. Engineering Mechanics, 2015, 32（6）:107-114 (in Chinese).

[29] Feng Zhou, Lu Li. Experimental sudy on hysteretic behavior of structural stainless steels under cyclic loading. Journal of Constructional Steel Research，122（2016）:94-109.

[30] AISC (2010), Seismic Provisions for Structural Steel Buildings, ANIS/AISC 341-10, Chicago.

[31] BSI (2005), Eurocode 3: Design of Steel Structures:Part 1-1: General Rules and Rules for Buildings, BSEN 1993-1-1, London.

[32] GB50011-2010, Code for seismic design of buildings. Beijing: China Architecture Industry Press, 2010. (in Chinese).

[33] GB/T 228.1-2010.MetallicMaterials-TensileTesting-Part1:Method of Test at Room temperature . Beijing: Standards Press of China, 2010 (in Chinese).

[34] JGT 101—96 Specification of testing methods for earthquake resistant building. Beijing:Chain Architecture & Building Press, 1997 (in Chinese).

[35] Nie J, Bai Y, Cai C S. New Connection System for Confined Concrete Columns and Beams. I: Experimental Study," ASCE Journal of Structural Engineering, 134(12): 1787-1799. Journal of Structural Engineering, 2008, 134(12):1787-1799.

Notation

A	section area
A^*	the percentage elongation after fracture
B	the width of the section
D_l	the displacement level corresponding to local buckling
D_{max}	the displacement levels corresponding to the maximum bearing capacity
D_u	the displacement levels corresponding to failure load
E_0	Elastic modulus
N	axial load
N_0	the axial-load ratio
L_0	actual height of the test specimen
P	The horizontal load
R_D	the readings of LVDT
E	the energy dissipation coefficient
P_{max}	peak load
P_u	85% of peak load
t	the thickness of the elements
$f_{0.2}$	the 0.2% proof stress
f_u	the ultimate tensile stress
n	strain-hardening exponents for the compound Ramberg–Osgood model
t_w	the thickness of the web
h	the height of the web
y	half the height of the section
δ_y	the yielding displacement
δ	the horizontal displacement
μ	The displacement ductility coefficient
Δ_y	lateral displacements at column yield
Δ_u	lateral displacements at column failure